Oxid Met (2017) 88:409–420
DOI 10.1007/s11085-017-9750-4

ORIGINAL PAPER

Effect of Yttrium as Alloying Element on a Model Alumina-Forming Alloy Oxidation at 1100 °C

Christophe Issartel[1] · Henri Buscail[1] · Sébastien Chevalier[2] · Jérôme Favergeon[3]

Received: 19 January 2017 / Published online: 8 March 2017

Abstract In order to study the effect of yttrium as alloying element on the high-temperature oxidation of an alumina-forming alloy, 0.093 wt% yttrium was incorporated into a model FeCrAl alloy. Yttrium has a beneficial effect on the isothermal oxidation behavior in air at 1100 °C. Glancing angle X-ray diffraction made on a sample oxidized for 1000 h under thermal cycling conditions indicated that yttrium is located at the internal interface as $Y_3Al_5O_{12}$. Secondary neutral mass spectrometry results showed that the diffusion mechanism is modified by the presence of yttrium as an alloying element. Moreover, the beneficial effect of yttrium on the alloy oxidation is also related to a reduced metallic grain size. The growth of metal grains during oxidation was especially observed on the yttrium-free FeCrAl alloy. It is also well established that the diffusion mechanism in the oxide scale is modified by yttrium. The aim of the present work was to show that yttrium also plays a role on the aluminum diffusion in the metallic substrate and has a strong influence on the kinetic transient stage during the FeCrAl–0.1Y oxidation.

Keywords Yttrium · Oxidation · FeCrAl · Alumina

✉ Christophe Issartel
christophe.issartel@udamail.fr

Henri Buscail
henri.buscail@udamail.fr

Sébastien Chevalier
sebastien.chevalier@u-bourgogne.fr

Jérôme Favergeon
jerome.favergeon@utc.fr

[1] LVEEM, Université d'Auvergne, 8 rue J.B. Fabre – CS 10219, 43009 Le Puy en Velay, France

[2] ICB, UMR 6030 CNRS, Univ. Bourgogne Franche-Comté, 21078 Dijon Cedex, France

[3] Roberval Laboratory, UMR 7337 CNRS, Université de Technologie de Compiègne, Centre de recherche de Royallieu, CS 60319, 60203 Compiègne, France

Introduction

The excellent oxidation resistance of FeCrAl alloys is due to the formation of a slow growing and adherent alumina scale. In order to increase the oxidation properties, reactive elements can be introduced in the alloy. The beneficial effect of rare earth element (REE) on the high-temperature oxidation of alloys has already been studied by several authors [1–6]. Previous works were generally conducted on industrial steels such as Kanthal AF [7, 8]. Nevertheless, in such alloys other minor elements could influence the oxidation resistance at high temperature. Sulfur can also show a bad influence on scale adherence [9, 10], introduction of small amount of magnesium induces $MgAl_2O_4$ formation in the outer part of the alumina scale [11], and titanium and zirconium have negative effects on the alloy lifetime [12]. It is thus interesting to investigate the specific effect of yttrium on the oxidation of an alumina-forming alloy by using a high-purity model substrate. A small amount of yttrium decreases the oxidation growth rate of alumina and increases the scale adhesion on the metallic substrate. The role of yttrium in the alloys depends upon its introduction mode. The beneficial effect is observed when yttrium is introduced in the alloy and not only deposited on the surface [13, 14]. After alumina-forming alloys oxidation, Zhenyu Liu has localized the RE along alumina grain boundaries [15–17]. Nevertheless, it is very difficult to observe yttrium located inside the oxide scale. Recently, Hellström et al. [18] explained that yttrium particles become incorporated into the scale during oxidation because of metal recession. Furthermore, the beneficial effect of yttrium is related to the suppression of the linear transient stage on kinetic curves. In order to better understand the role of yttrium, the oxidation of model alumina-forming alloys at 1100 °C has been followed by several analytical techniques such as X-ray diffraction; thermogravimetric analysis; glow discharge optical emission spectrometry.

Experimental Procedures

The two materials investigated in this study are model alumina-forming alloys. Each alloy composition is given in Table 1. In order to study the effect of yttrium as alloying element, 0.093 wt% yttrium was incorporated into the model FeCrAl alloy to give the FeCrAl–0.1Y substrate. The high-purity FeCrAl and FeCrAl–0.1Y alloy elaborated by fusion of the metallic elements under vacuum. The ingot was transformed into a cylindrical bar by forging. They were provided by Pr J. Le Coze (Ecole des Mines de Saint-Etienne, France), and the analyses were made by optical emission spectroscopy (OES).

Table 1 FeCrAl and FeCrAl–0.1Y alloy composition in wt%

wt%	Fe	Cr	Al	C	S	O	N	Y
FeCrAl	Bal.	19.98	5.00	<0.001	<0.001	<0.001	<0.001	–
FeCrAl–0.1Y	Bal.	19.70	5.00	<0.001	<0.0005	<0.001	<0.001	0.093

One-mm-thick cylindrical specimens of around 2 cm^2 total surface area were cut from the metallic bars. The specimens were abraded up to the 600-grit SiC paper, then degreased with acetone and finally dried.

In this paper, 1100 °C is the only studied temperature. Various experiments have been realized as follows: (a) Isothermal oxidation testing was performed during 100 h at 1100 °C in air under the atmospheric pressure using a Setaram TGDTA 92-1600 microthermobalance. (b) For secondary neutral mass spectrometry (SNMS) examination, samples were oxidized by 200 mBar $^{16}O_2$, during 2 h in a first time, and then 200 mBar $^{18}O_2$ was introduced during 4 h without stopping experiment. The SNMS examination of the oxide scale was carried out using a VG instrument, with an Ar^+ sputter energy of 10 keV under a 45° incidence angle. (c) Oxidation during 4 h in furnace in air was conducted. The microstructure and elemental distribution in the oxide scales were analyzed by scanning electron microscopy (SEM), energy-dispersive X-ray spectrometry (EDX) and glow discharge optical emission spectrometry (GDOES). After the 4-h oxidation, some specimens have been polished until the oxide scale has been removed and the alloy microstructure has been observed and compared to the non-oxidized alloys. (d) Cyclic oxidation (20 h at 1100 °C and 4 h at 20 °C) was made during 1000-h oxidation time and glancing angle XRD (GAXRD) was used to analyze the scale composition from the gas-oxide interface to the oxide-metal interface. (e) In situ X-ray diffraction was followed by the acquisition of a pattern every hour during the 40-h test at 1100 °C. In situ patterns were obtained with a high-temperature Anton PAAR HTK 1200 chamber installed in a Philips X'pert MPD diffractometer (CuKα1 = 0.15406 nm radiation).

Results

Kinetic Results

Mass gain per unit area versus time curves ($\Delta m/A = f(t)$) of alloys without Y- and yttrium-containing specimens oxidized during 100 h at 1100 °C, in air, are reported in Fig. 1. The comparison of the kinetic curves shows that the FeCrAl sample has a higher weight gain during the 100-h oxidation. The introduction of yttrium as alloying element has a beneficial effect on the oxidation rate since the weight gain is remarkably reduced all over the 100 h of the test. The calculation of the parabolic rate constants, from the slope of ($\Delta m/A = f(\sqrt{t})$ [19], evidences that the oxidation rate is close to each other (Table 2). For the specimen without *Y*, the first hours of oxidation have been neglected because a transient linear stage occurs before the parabolic behavior.

SEM and Optical Micrographic Observations

Substrates micrographs of the specimens have been made before and after 4-h oxidation in air at 1100 °C (Fig. 2). After the 4-h oxidation, the specimens have been polished until the oxide scale has been removed. Results show a larger grains

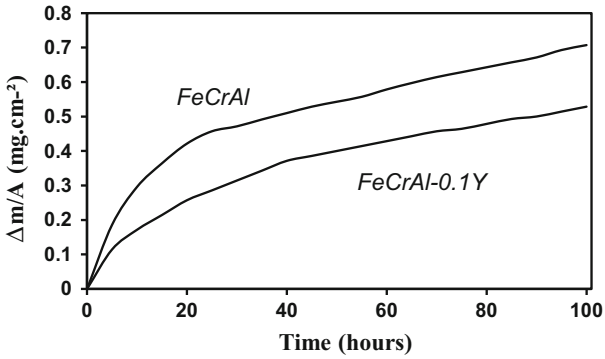

Fig. 1 Mass gain versus time curves of yttrium alloyed and alloys without Y at 1100 °C, in air

Table 2 Parabolic rate constants of specimens oxidized at 1100 °C in air

Sample	FeCrAl	FeCrAl–0.1Y
k_p (g^2 cm^{-4} s^{-1})	1.1×10^{-12}	9.6×10^{-13}

size for the FeCrAl sample than FeCrAl–0.1Y sample before oxidation. Results also show that temperature of 1100 °C increases the grains size of FeCrAl sample (grains size increases by a factor of 8) The same temperature has not much influence on substrate grains size of FeCrAl–0.1Y sample (factor 1.7). On the yttrium-containing alloy (FeCrAl–0.1Y) results show that yttrium inhibits the growth of metallic grain size. The grain sizes are listed in Table 3.

SEM observation and EDXS analysis have not permitted the detection of yttrium in the oxide scale. Nevertheless, yttrium has been detected in the substrate before oxidation and in the metallic substrate under the scale obtained after 4-h oxidation in air (Fig. 3). Before and after oxidation, the white particles are composed of pure yttrium. In both cases, they cannot be detected by XRD due to their low ratio in the alloy.

SNMS Results

On FeCrAl specimens, the SNMS results exhibit that after the two-stage experiment most of the new oxide formed with ^{18}O is located at the external interface (Fig. 4a). This means that the oxide growth mechanism implies a major cationic diffusion contribution. The ^{18}O profile also indicates that some new oxide is formed in the pre-existing $Al_2^{16}O_3$ scale close to the internal interface. A little contribution of oxygen inward diffusion must also be considered.

On the yttrium-containing alloy (FeCrAl–0.1Y), the SNMS profiles show that the ^{18}O peak is concentrated at the bottom of the pre-formed alumina scale, indicating then that the new oxide is formed at the internal interface (Fig. 4b). The alumina

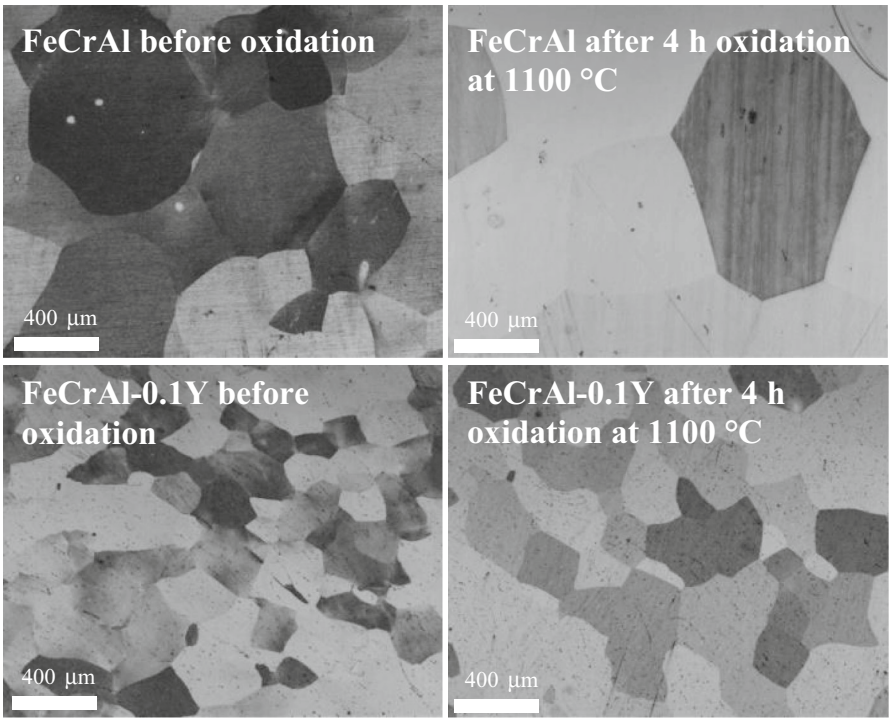

Fig. 2 Optical micrographs of yttrium alloyed and non-alloyed specimens

Table 3 Grain sizes of yttried and non-yttried specimens oxidized 4 h at 1100 °C in air

Sample	FeCrAl		FeCrAl–0.1Y	
Oxidation time	0 h	4 h	0 h	4 h
Average grain size (μm^2)	186×10^3	1630×10^3	31×10^3	54×10^3

scale is therefore growing by a predominant inward anionic diffusion process. The yttrium is mainly detected and seems to be located at the internal interface.

X-Ray Diffraction

On alloys without Y, in situ X-ray diffraction shows the growth of a α-Al_2O_3 scale (ICDD 46-1212) during the first 40-h oxidation at 1100 °C, in air. For the FeCrAl–0.1Y specimens, all along the 40-h oxidation, no yttrium oxides could be detected. As observed on alloys without Y, α-Al_2O_3 is the only oxide growing on the substrate. Nevertheless, we have noticed some differences concerning the relative diffraction peak intensities observed. In both cases, we can well identify α-Al_2O_3,

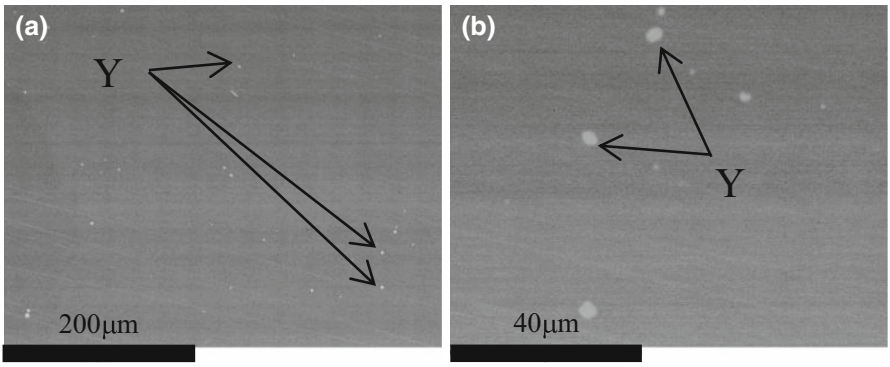

Fig. 3 SEM obtained on FeCrAl–0.1Y surfaces **a** before oxidation and **b** after 4-h oxidation at 1100 °C

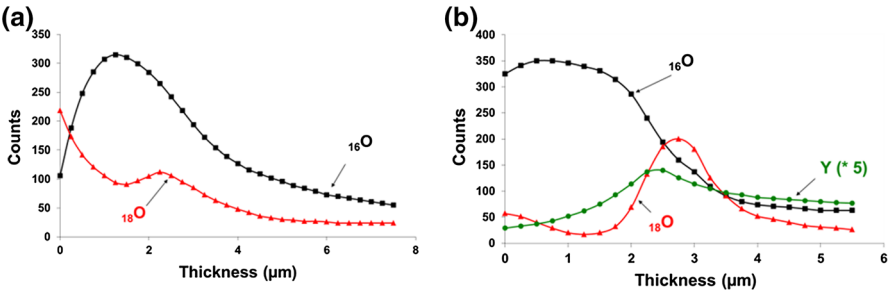

Fig. 4 SNMS results on **a** FeCrAl and **b** FeCrAl–0.1Y samples oxidized at 1100 °C during 2 h in 200 mBar $^{16}O_2$, followed by 4 h in 200 mBar $^{18}O_2$

but it appears that this oxide grows following two different crystallographic orientations depending on the presence of yttrium.

After 1000 h of thermal cyclic oxidation tests, no spallation was observed on the FeCrAl–0.1Y alloy, and the analysis by glancing angle X-ray diffraction at various incident angles are performed to obtain more precise information on the scale structure (Fig. 5). On the θ–2θ pattern at normal incidence, the X-ray penetration depth is maximal and we can observe the α-Al_2O_3 and $Y_3Al_5O_{12}$ peaks. The pattern obtained at 2° incidence shows that all the peak intensities decrease but this effect is more pronounced for the $Y_3Al_5O_{12}$ peaks. This result would indicate that $Y_3Al_5O_{12}$ is localized close to the scale-metal interface.

GDOES Results

Figure 6 shows the GDOES depth profiles for elemental distributions in the scales formed by oxidization for 4 h at 1100 °C in air. The scale/substrate interface is assumed to be located at the depth where the Fe profile increases, near 3 μm. The profiles indicate that the scales formed on the yttried and non-yttried samples were composed of an alumina layer. Nevertheless, it can be observed a more important chromium presence on the top of the alumina layer for FeCrAl–0.1Y. The profiles

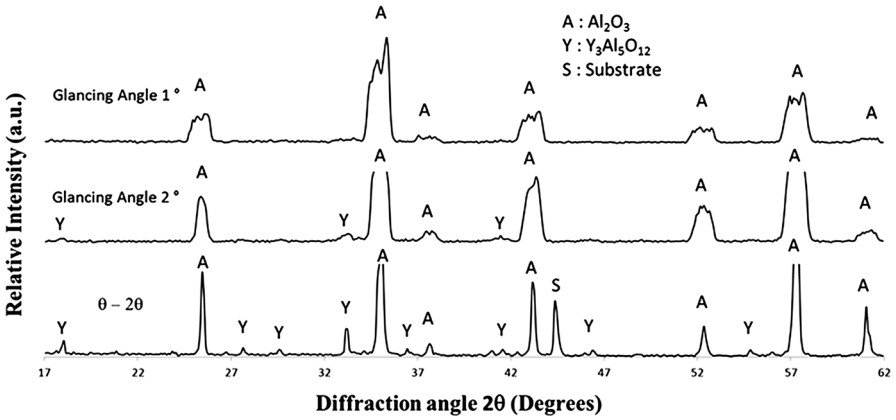

Fig. 5 Main glancing angle X-ray patterns obtained on yttrium alloying FeCrAl, oxidized at 1100 °C, in air, during 1000 h of cyclic oxidation

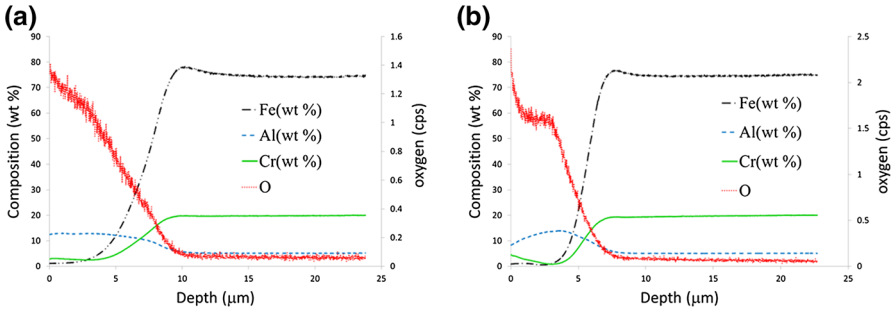

Fig. 6 GDOES depth profiles for the scales formed by oxidation for 4 h at 1100 °C in air: **a** FeCrAl, **b** FeCrAl–0.1Y

also indicate that diffusion of aluminum is not the same in the two samples. The flat profile of aluminum on the FeCrAl proves that diffusion rate is fast enough in the substrate to supply the scale with aluminum. For the FeCrAl–0.1Y sample, the aluminum and oxygen profiles indicate that diffusion of Al is less important than diffusion of oxygen. The decrease in aluminum diffusion rate is shown in the scale, but it is also true in the metallic substrate.

Discussion

On FeCrAl specimens oxidized at 1100 °C, in situ XRD shows that only α-Al_2O_3 is formed all along the oxidation process. α-Al_2O_3 is the only oxide observed during the transient oxidation stage. This result can be related to other works which have shown that α-Al_2O_3 is the only oxide detected on oxidized FeCrAl specimens after cooling to room temperature [15, 20, 21]. On the FeCrAl–0.1Y alloy, yttrium oxides are not detected by in situ X-ray diffraction after 40-h oxidation.

The SNMS examination of the oxide scale shows that a mixed diffusion process occurs on the model alumina-forming alloy oxidized at 1100 °C (Fig. 4a), whereas a predominant inward oxygen diffusion process is observed in the case of yttrium-containing specimens (Fig. 4b). The mixed diffusion process promotes ridges formation and a less protective and adherent scale as proposed by Pint et al. [8]. The change in the diffusion mechanism is a consequence of the yttrium presence, and an improvement of the corrosion resistance for the FeCrAl–0.1Y alloy is observed.

In Fig. 6, glancing angle XRD results show that $Y_3Al_5O_{12}$ is present close to the internal interface. But the presence of $Y_3Al_5O_{12}$ at this interface cannot explain the change in diffusion mechanism because $Y_3Al_5O_{12}$ is only observed after long-term oxidation, as it is the case during 1000-h thermal cycling tests. $Y_3Al_5O_{12}$ could not be detected by in situ XRD after 40-h oxidation. It seems to be mainly located at the internal interface. $Y_3Al_5O_{12}$ belongs to the garnet YAG oxide type structure, and this oxide has been described by other authors [22–24]. As proposed by Liu or Wood [15, 20], yttrium is probably located at the oxide grain boundaries. It is also mentioned that $Y_3Al_5O_{12}$ is often found segregated along the α-Al_2O_3 grain boundaries [25–27].

Yttrium is not easily observed in the alumina scale, but it is detected in the metallic substrate. Figure 3 clearly exhibits that yttrium is still present under the scale after 4-h oxidation. In light of the anionic diffusion mechanism, Hellström et al. [18] explained that the yttrium particles can be incorporated into the scale during oxidation because of metal recession.

Isothermal kinetic results (Fig. 1) have shown that alloys without Y have a higher weight gain compared to FeCrAl–0.1Y samples after 100-h oxidation at 1100 °C in air. But it cannot be explained by the presence of yttrium in the scale because we have shown that it takes time for yttrium to be introduced inside the oxide scale. The FeCrAl–0.1Y sample follows a parabolic growth rate from the beginning of the oxidation test, contrarily to the FeCrAl sample which presents a transient linear stage. It then appears that yttrium plays a role but it cannot act inside the alumina scale at the early stage of oxidation.

Huntz [28] proposed that the oxide scale growth is controlled by "the slowest process of dominant route", i.e., the slowest step of the fastest route. This author considers two routes: route 1 which considers the cation process and route 2 which considers the anion process. The possible limiting steps applied to this study are listed Table 4:

Generally, the fast reactions of adsorption are not considered to be the limiting steps. Thus, if the oxide scale growth is controlled by one (or several) diffusional phenomena (route 1 or 2), the oxidation rate behavior is parabolic. And if the oxide scale growth is controlled by a chemical reaction, a linear rate behavior is observed.

Concerning the FeCrAl–0.1Y sample kinetic curve, a parabolic rate behavior is followed from the beginning of the test. No transient stage is observed. It indicates that a diffusional process controls the oxide scale growth. Before the formation of a continuous Al_2O_3 scale, Al or O diffusion in alumina cannot be the limiting step of the oxide scale growth. If the limiting step of the cationic and anionic routes cannot be the aluminum or oxygen diffusion in alumina, then it should be the Al diffusion in the alloy. It corresponds to the first step of route 1 (Table 4) and this process

Table 4 Limiting step of oxide scale growth

Route 1	Route 2
Al diffusion in FeCrAl	$O_2 \rightarrow 2O_{ads}$
$Al \rightarrow Al^{3+} + 3e^-$	$O_{ads} + 2e^- \rightarrow O^{2-}$
Al diffusion in Al_2O_3	O diffusion in Al_2O_3
$2Al^{3+} + 3O_{ads} \rightarrow Al_2O_3$	$3O^{2-} + 2Al \rightarrow Al_2O_3$

controls the initial oxide scale growth before the establishment of a continuous alumina scale. This is a diffusional step and this corresponds to the parabolic rate law followed from the beginning of the test (Fig. 1). According to the yttrium-free FeCrAl oxidation kinetic curve (Fig. 1), a transient linear stage is observed. In this case, the Al diffusion in the substrate is fast enough and cannot be the limiting step of route 1. The chemical reaction between aluminum and oxygen controls the oxide scale growth during the transient stage, before the formation of a continuous Al_2O_3 scale.

After the transient stage, a continuous alumina scale is formed on both alloys. A diffusional process leads to a parabolic behavior. The k_p values measured on the FeCrAl and FeCrAl–0.1Y are close to each other (Table 2). It indicates that similar limiting diffusion processes are involved through the alumina scales. Figure 4b emphasizes the fact that the alumina scale grows by an inward anionic diffusion process on the FeCrAl–0.1Y alloy. The aluminum diffusion in alumina is slightly faster than oxygen diffusion in alumina. At 1100 °C, Le Gall has found that $D_{Al}/D_O = 24$, with D_{Al} and D_O, respectively, the diffusion coefficients of aluminum and oxygen in an alumina scale [29]. The anionic oxygen diffusion in alumina scale is therefore considered as the limiting step.

On the FeCrAl–0.1Y alloy, the presence of chromium (Fig. 6b) in the outer part of the scale can be explained by the process involved during the transient stage. With the measurement of Al diffusion in an yttried metallic substrate, Lesage exhibited that there is a competition between the oxidation rate governed by the oxygen diffusion through the oxide scale to the oxide/metal interface and the diffusion of aluminum in the substrate to the metal/oxide interface [30]. In the present work, the low aluminum diffusion rate in the yttried substrate allows the chromium oxidation during the transient stage (Fig. 6b). After the transient stage, as long as the process is governed by anionic diffusion, the chromium stays close to the outer part of the scale. This is in accordance with what is proposed by other authors who indicate that the Al_2O_3 scale structure corresponds to an outward growing of Al_2O_3; a continuous Cr-rich zone; and an inner layer of pure α-Al_2O_3 [7–31]. The interface between the two alumina subscales corresponds to the original metal surface, and chromium is incorporated in this zone during the transient oxidation stage [18]. The textures of both alumina scales have been discussed by several authors. The duplex structure of alumina is made of equiaxed grains in the external part and columnar alumina grains in the inner one [32]. The anionic and cationic diffusions contribute to the scale development (Fig. 4a), and an equiaxed grain morphology of the scale is observed [33].

Our results show that yttrium acts on the Al diffusion in the metallic substrate. Lesage [30] has shown that at relatively low temperatures (1000–1080 °C), oxygen diffuses faster in alumina than aluminum in an yttried substrate. And above 1080 °C, the diffusion rate of Al increases faster than oxygen in the scale. In Lesages's work, the 1080 °C temperature corresponds to the intermediate temperature between the aluminum atoms flow and the oxygen flow at the metal/oxide interface. But the alloy microstructure consists of large centimetric elongated grains. It means that the contribution of grain boundary diffusion is negligible. Our results show that the FeCrAl–0.1Y alloy microstructure of is not the same compared to the FeCrAl one (Fig. 2). Yttrium appears to block the alloy grain growth during oxidation and decreases the aluminum diffusion in the metallic substrate. Metal grains remain smaller, and thus, the number of grain boundaries remains relatively high.

The apparent diffusion coefficient can be calculated following Eq. (1):

$$D_{\text{app}} = (1 - f)D_{\text{sb}} + f\,D_{\text{gb}} \tag{1}$$

D_{sb} and D_{gb} are, respectively, the substrate and grain boundary diffusion coefficients and f is the volume fraction of grain boundaries: $f = 3\delta/\varphi$ where δ is the grain boundary width and Φ is the diameter of the grains.

If the grain size is small, f increases and D_{gb} is more influent in the expression of D_{app}. In this study, yttrium favors grain boundary aluminum diffusion in the alloy. Results show that yttrium also decreases D_{app}. D_{gb} is certainly lower in the Y-containing FeCrAl than in the FeCrAl without yttrium. It is probably also right for D_{sb}. If D_{app} of aluminum in Fe [34], FeCrAl [35] and FeCrAlY [30] have been measured, the contribution of grain boundaries was never discussed.

Yttrium is well known to improve the alumina scale adherence. The influence of the alloy grain size can also be considered. Horibe and Nakayama [36] have already stated that on a Fe–18Cr alloy the grain growth of the ferrite might promote the disruption of the initial oxide. Sasa and Nakayama [37] confirms that grain growth contribute to the breakaway and subsequent abnormal oxidation for a Fe–17Cr at 1000 °C. Several authors have observed the influence of average grain size of the metal on oxidation and scale adherence [38–42]. In the present work (Fig. 2) shows that the alloy grain growth is especially observed on the FeCrAl and the scale adherence is much better on FeCrAl–0.1Y.

Conclusions

The present work shows that on the yttrium-containing alloy (FeCrAl–0.1Y) the alumina scale is growing by a predominant inward anionic diffusion process which leads the formation of a more protective and adherent scale. The role of yttrium is to block the alloy grain growth during oxidation and decreases the aluminum diffusion in the alloy. The duplex structure of the alumina scale corresponds to an external thin equiaxed subscale and an inner columnar one. The interface between the two layers of alumina has been reported to correspond to the original metal surface, and

chromium is incorporated in this zone during the transient oxidation stage. Yttrium is well known to improve the adherence of alumina scales. This work shows that the oxidation mechanism is also related to the influence of yttrium on the alloy grain size.

Acknowledgements The authors thank Prof. J. Le Coze for providing the model base FeCrAl and FeCrAl0.1Y alloys. They are also grateful to Prof. G. Borchardt and Dr. Strehl for the $^{16}O_2$ and $^{18}O_2$ oxidations, and Prof. S. Weber for the SNMS experiments.

References

1. K. Messaoudi, A. M. Huntz and B. Lesage, *Materials Science and Engineering A* **247**, 248 (1998).
2. J. Jedlinski, *Oxidation of Metals* **39**(1/2), 55 (1993).
3. S. Chevalier, G. Strehl, H. Buscail, G. Borchardt and J. P. Larpin, *Materials and Corrosion* **55**, 352 (2004).
4. X. G. Zheng and D. J. Young, *Corrosion Science* **40**(4/5), 741 (1998).
5. K. Przybylski and G. J. Yurek, *Materials Science Forum* **43** 1 (1989).
6. P. Castello, F. H. Stott and F. Gesmundo, *Corrosion Science* **41**, 901 (1999).
7. R. Cueff, H. Buscail, E. Caudron, C. Issartel and F. Riffard, *Corrosion Science* **45**, 1815 (2003).
8. B. A. Pint, A. J. Garatt-Reed and L. W. Hobbs, *Materials at High Temperatures* **13**, 3 (1995).
9. T. Amano, T. Watanabe and M. Michiyama, *Oxidation of Metals* **53**, 451 (2000).
10. R. Bousquet, D. Fayeulle, E. Bruyere and F. Bertrand, *Oxidation of Metals* **80**, 13 (2013).
11. P. Untoro, M. Dani, H. J. Klaar, J. Mayer, D. Naumenko, J. C. Kuo, and W. J. Quadakkers, *Materials Aspects in Automotive Catalytic Converters*, 271 (2002).
12. D. Naumenko, J. Le-Coze, E. Wessel, W. Fischer and W. J. Quadakkers, *Materials Transactions* **43**, 168 (2002).
13. S. Chevalier, A. P. Dawah Tankeu, H. Buscail, C. Issartel, G. Borchardt and J. P. Larpin, *Materials and Corrosion* **55**, 610 (2004).
14. S. Chevalier, G. Strehl, H. Buscail, C. Issartel, G. Borchardt and J. P. Larpin, *Materials and Corrosion* **57**, 476 (2006).
15. Z. Liu, W. Gao and Y. He, *Oxidation of Metals* **53**(3/4), 341 (2000).
16. K. Przybylski, A. J. Garratt-Reed and G. J. Yurek, *Journal of the Electrochemical Society* **135**, 509 (1988).
17. K. Bongartz, W. J. Quadakkers, J. P. Pfeifer and J. S. Becker, *Surface Science* **292**, 196 (1993).
18. K. Hellström, N. Israelsson, N. Mortazavi, S. Canovic, M. Halvarsson, J. E. Svensson and L. G. Johansson, *Oxidation of Metals* **83**, 533 (2015).
19. B. Pieraggi, *Oxidation of Metals* **27**, 177 (1987).
20. G. C. Wood and F. H. Stott, in *High Temperature Corrosion*, Nace-6, eds. R. A. Rapp (NACE International, 1958), p. 227.
21. R. Prescott and M. J. Graham, *Oxidation of Metals* **38**(1/2), 73 (1991).
22. K. M. N. Prasanna, A. S. Khanna, R. Chandra and W. J. Quadakkers, *Oxidation of Metals* **46**(5/6), 465 (1996).
23. E. Schumann, *Oxidation of Metals* **43**(1/2), 157 (1995).
24. R. Cueff, H. Buscail, E. Caudron, and F. Riffard, *La revue de Métallurgie-SF2M* **147** (2000).
25. M. K. Loudjani, C. Haut and S. Parisot, *Radiation Effects and Defects in Solids* **134**, 233 (1995).
26. M. K. Loudjani and C. Haut, *Journal of the European Ceramic Society* **16**, 1099 (1996).
27. B. A. Pint, *Oxidation of Metals* **45**(1/2), 1 (1996).
28. A. M. Huntz, *Journal de Physique III* **5**, 1729 (1995).
29. M. Le Gall, A. M. Huntz, B. Lesage, C. Monty and J. Bernardini, *Journal of Materials Science* **30**, 201 (1995).
30. B. Lesage, L. Maréchal, A. M. Huntz and R. Molins, *Defect and Diffusion Forum* **194–199**, 1707 (2001).
31. F. Liu, M. Halvarsson, K. Hellström, J. E. Svensson and L. G. Johansson, *Oxidation of Metals* **83**, 441 (2015).

32. S. Chevalier, J. P. Larpin, P. Dufour, G. Strehl, G. Borchardt, K. Przybylski, S. Weber and H. Scherrer, *Materials at High Temperatures* **20**(3), 365, (2003).
33. J. R. Blachère, E. Schumann, G. H. Meier and F. S. Pettit, *Scripta Materialia* **49**, 909 (2003).
34. I. A. Akimova, V. M. Mironov and A. V. Pokoyev, *Fiz. Metal. Metalloved* **56**(6), 1225 (1983).
35. A. Heesemann, E. Schmidtke, F. Faupel, A. Kolb-Telieps and J. Klöwer, *Scripta Materialia* **40**(5), 517 (1999).
36. S. Horibe and T. Nakayama, *Corrosion Science* **15**, 589 (1975).
37. K. Sasa and T. Nakayama, *Corrosion Science* **17**, 783 (1977).
38. M. D. Merz, *Metallurgical Transactions* **10A**, 71 (1979).
39. S. N. Basu and G. J. Yurek, *Oxidation of Metals* **36**(3/4), 281 (1991).
40. I. Murris, Y. P. Jacob, V. A. C. Haanappel and M. F. Stroosnijder, *Oxidation of Metals* **55**(3/4), 307 (2001).
41. X. Peng, J. Yan, Y. Zhou and F. Wang, *Acta Materialia* **53**, 5079 (2005).
42. J. H. Kim, D. I. Kim, S. Suwas, E. Fleury and K. W. Yi, *Oxidation of Metals* **79**, 239 (2013).